Faraday
Discussions

Accepted Manuscript

**Faraday
Discussions**

**Royal Society of
Chemistry**

ROYAL SOCIETY
OF CHEMISTRY

ROYAL SOCIETY
OF CHEMISTRY

www.rsc.org/faraday_d

Ab initio modeling of the bonding of benzotriazole corrosion inhibitor to reduced and oxidized copper surfaces

Anton Kokalj[*][a]

The bonding of benzotriazole—an outstanding corrosion inhibitor for copper—on reduced and oxidized copper surfaces is discussed on the basis of density functional theory (DFT) calculations. Calculations reveal that benzotriazole is able to bond with oxide-free and oxidized copper surfaces and on both of them it bonds significantly stronger to coordinatively unsaturated Cu sites. This suggests that benzotriazole is able to passivate the reactive under-coordinated surface sites that are plausible microscopic sites for corrosion attack. Benzotriazole can adsorb in a variety of different forms, yet it forms a strong molecule–surface bond only in deprotonated form. The bonding is even stronger when deprotonated form is incorporated into organometallic adcomplexes. This is consistent with existing experimental evidence that benzotriazole inhibit the corrosion by forming protective organometallic complexes. It is further shown that adsorption of benzotriazole considerably reduces the metal work function, which is a consequence of large permanent molecular dipole and properly oriented adsorption structure. It is argued that such a pronounced effect on the work function is of importance for corrosion inhibition, because it should *diminish* the anodic corrosion reaction, which is consistent with existing experimental evidence that benzotriazole, although a mixed type inhibitor, predominantly affects the anodic reaction.

1 Introduction

There are various ways of corrosion protection and one of them is by means of corrosion inhibitors, which are substances that have the ability to considerably slow down the corrosion of metals and alloys by decreasing the rate of corrosion processes. Among efficient corrosion inhibitors are also organic molecules. It is commonly believed that strong interaction between organic inhibitor molecule and a substrate is very important for achieving the inhibitory effect.[1–3] In particular, Bockris stated that *organic molecules must be adsorbed to become inhibitors*.[3] Despite the soundness of the *strong adsorption* premise, DFT (density

[a] *Department of Physical and Organic Chemistry, Jožef Stefan Institute, Jamova 39, SI-1000 Ljubljana, Slovenia; Fax: +386-1-477-3822; Tel: +386-1-477-2523; E-mail: tone.kokalj@ijs.si; URL: http://www.ijs.si/ijsw/K3-en/Kokalj*

functional theory) calculations have revealed—contrary to what might have been intuitively expected—that some outstanding inhibitor molecules, such as benzotriazole and several other azoles, interact only weakly in its intact form with substrates.[4–6] For example, intact benzotriazole molecule bonds only by about 0.5 eV to Cu(111) surface,[5,6] which is similar in strength to solvation interaction between benzotriazole and water.[7,8] This implies that the net adsorption energy at the water/solid interface should be rather small, which may seem surprising, because if the bonding is that weak then aggressive corrosive species would easily replace benzotriazole from the surface (if it would adsorb at all). How then, can benzotriazole act against corrosion?

Benzotriazole has been used for a long time as one of the most efficient copper corrosion inhibitors[1,9–11] and there are numerous studies of its inhibition action on copper. Despite the bulk of literature, Finšgar and Milošev stated in a recent review:[11] "... *the exact mechanism of benzotriazole action on copper materials still remains to be elucidated. It is important to clarify why benzotriazole, and not other organic molecules with similar electronic structure, imparts corrosion protection. The answer to this question will provide the basis for predicting new and more effective corrosion inhibitors.*"

The aim of this paper is to discuss the adsorption behavior of benzotriazole—as elucidated by DFT calculations—on reduced and oxidized copper surfaces (for the latter only the Cu(I) oxidation state is currently considered). The issue seems relevant, because controversial suggestions exist in the literature,[11] *i.e.*, according to some researchers the presence of oxides is important,[12–14] while others claimed that their presence is not needed for the adsorption of benzotriazole.[15,16] It has to be emphasized that adsorption behavior is not synonymous with the mechanism of corrosion inhibition, yet it may nevertheless provide some useful information and insight. The literature is replete with numerous suggestions about possible adsorption mechanisms of benzotriazole on copper.[11] There are at least two reasons of why this is so: the first is due to complexity of the investigated system. The interpretation of experimental data therefore involves various degree of assumptions and different assumptions may lead to different conclusions. The second reason is due to—as is argued in this paper—nontrivial adsorption behavior of benzotriazole, because it can adsorb in a variety of different forms. It all depends on the details and perhaps this is one of the strengths of benzotriazole and other inhibitor molecules; depending on different conditions they will adopt one of the several possible forms and thus sustain various situations.

There are several important points to keep in mind when considering the results presented in this paper. The most important is that due to obvious modeling reasons the presented results refer to the solid/vacuum interface (solvent effect are estimated posteriory when explicitly stated so), whereas in the context of corrosion the solid/water is the relevant interface. Apart from the fact that solvent considerably affects the energetics of adsorption, there is another distinction between the adsorption at solid/vacuum and solid/water interfaces. The adsorption at the latter is competitive (or substitutional), because the surface is always covered with solvent molecules and other possible species. So a given molecule will adsorb only if its adsorption is competitive enough to substitute other species from the surface. In contrast, at the solid/vacuum interface the surface is clean and the molecule adsorbs readily (say that surface temperature is low enough)

unless its interaction with the surface is repulsive.

The paper is organized as follows: section 2 contains a brief description of computational method along with some definitions, while section 3 deals with bare metallic copper surfaces and reviews the pertinent computational DFT studies. These data are put into a new context and the relevance of the work function reduction upon adsorption of inhibitor is emphasized. Oxidized copper surfaces are considered in section 4, where significant new results are presented. Section 5 finally contains the conclusions.
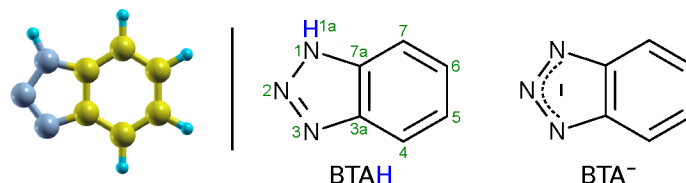
Scheme 1 Skeleton structures of neutral BTAH (middle) and its deprotonated BTA⁻ form (right). Numbering of atoms is also indicated. Ball-and-stick model of BTAH is shown on the left to indicate the respective atom coloring.

2   Technical details

Definitions. Term "copper surface" shall implicitly indicate the bare (reduced) metallic copper surface (oxidation state of 0); oxidized surface shall be explicitly referred to as "oxidized". The labels BTAH and BTA indicate the intact and dissociated (without H1a atom/proton) benzotriazole molecule, respectively (atom numbering and skeleton structures of neutral BTAH molecule and deprotonated BTA⁻ anion are shown in Scheme 1). $BTAH_{(g)}$, $BTAH_{(solv)}$, $BTAH_{(ads)}$ stand for gas-phase, solvated, and adsorbed molecule, respectively (and analogously for other species). Notation BTA–Cu refers to organometallic complex, while the standalone chemisorbed form is designated as $BTA_{(ads)}$. Other labels are defined when first used.

Computational. DFT calculations were performed with the plane-wave pseudo-potential method as implemented in the `PWscf` code from the `Quantum ESPRESSO` distribution,[17] using the ultrasoft pseudopotentials[18] and plane wave basis set with kinetic energy cutoff of 30 Ry (240 Ry for the charge-density), while molecular graphics were produced by the `XCRYSDEN`[19] graphical package. Calculations were performed with PBE[20] and reparametrized PBE-D' energy functionals; the former was used for chemisorption and the latter for parallel physisorption modes. PBE-D' includes a semi-empirical dispersion correction of Grimme,[21,22] which was reparametrized[23] to match the experimental adsorption energy of benzene on Cu(111). Cu surfaces were modeled by periodic slabs with the in-plane lattice spacing fixed at the calculated equilibrium Cu bulk lattice parameter (3.67 Å for PBE[24] and 3.64 Å for PBE-D'[23]). For Cu₂O surfaces, the PBE calculated equilibrium bulk lattice parameter of 4.35 Å was used. Spin polarization was used when needed. For further computational details see our previous publications, in particular ref. 8 and also ref. 7.

Molecular adsorption energies (at solid/vacuum interface) were calculated as:

$$E_{\text{ads}} = E_{\text{A/surf}} - (E_{\text{surf}} + E_{\text{A}}). \tag{1}$$

where the subscript A stands for adsorbate; E_{A}, E_{surf}, and $E_{\text{A/surf}}$ are the total energies of isolated adsorbate (molecule or atom), Cu or Cu_2O slab, and adsorbate/slab system, respectively. The use of charged species was avoided in calculations employing periodic boundary conditions, where the long range Coulomb interactions dictate the use of charge neutrality. The adsorption (binding) energies of deprotonated BTA^-, Cl^-, and H^+ are therefore calculated with respect to isolated radicals ($BTA^\odot$, Cl, and H) and are designated as $E_{\text{b}}^\odot$. Symbol $\odot$ is used to indicate the radical nature of the initial state. Subscript "b" is used in favor of "ads" to remind that binding energy of $BTA_{\text{(ads)}}$ is measured with respect to isolated $BTA^\odot$ (and not BTAH) and that of $Cl_{\text{(ads)}}$ and $H_{\text{(ads)}}$ with respect to isolated Cl and H (and not Cl_2 and H_2 molecules). The $E_{\text{b}}^\odot$ therefore measures the binding energy of these radicals to the surface. On metal surfaces, the binding energy can be recalculated with respect to anion in the initial state as: $E_{\text{b}}^{(-)} = E_{\text{b}}^\odot + \text{EA}^\odot - \Phi$, where $\text{EA}^\odot$ is the electron affinity of corresponding radical and Φ is a work function (for cations the equation is: $E_{\text{b}}^{(+)} = E_{\text{b}}^\odot - \text{IP}^\odot + \Phi$, where $\text{IP}^\odot$ is the ionization potential or respective radical). Analogously to $E_{\text{b}}^\odot$, also the E_{ads} of $BTAH_{\text{(ads)}}$ is occasionally labeled as E_{b}, in particular, when the molecule–surface binding is of primary concern.

3 Adsorption of benzotriazole on reduced copper surfaces: bare Cu(*hkl*) and defects thereon

Adsorption structures of benzotriazole on bare copper surfaces have been studied in detail by means of DFT calculations.[5–8,23,25–28] The main findings of these studies are briefly explained below (section 3.1 and, in part, also 3.2) as to make a proper context for the current discussion paper.

3.1 Description of various DFT identified adsorption modes

Benzotriazole can adsorb either molecularly as $BTAH_{\text{(ads)}}$ or dissociatively as $BTA_{\text{(ads)}} + H_{\text{(ads)}}$ (cleavage of N1–H bond). While the $BTAH_{\text{(ads)}}$ bonds weakly, the $BTA_{\text{(ads)}}$ is strongly chemisorbed on copper surfaces. The calculated activation energy of dissociation for weakly chemisorbed BTAH is about 1.1 eV on Cu(111), but on more open surfaces and step-edge defects the activation energy decreases bellow 1 eV.[27] Dissociative adsorption of benzotriazole is experimentally well established, because it has been often observed that the H1a atom of benzotriazole is removed upon chemisorption on copper surfaces even under ultra high vacuum conditions.[15,28–31]

Structures of different identified adsorption modes of $BTAH_{\text{(ads)}}$ and $BTA_{\text{(ads)}}$ are shown in Fig. 1 and binding energies as a function of coordination number of surface Cu atoms involved in the adsorption site are shown in Fig. 2.

3.1.1 Adsorption forms of $BTAH_{\text{(ads)}}$. BTAH can either weakly chemisorb in an upright geometry ($BTAH_\perp$) via triazole nitrogen atoms with the N–Cu dis-
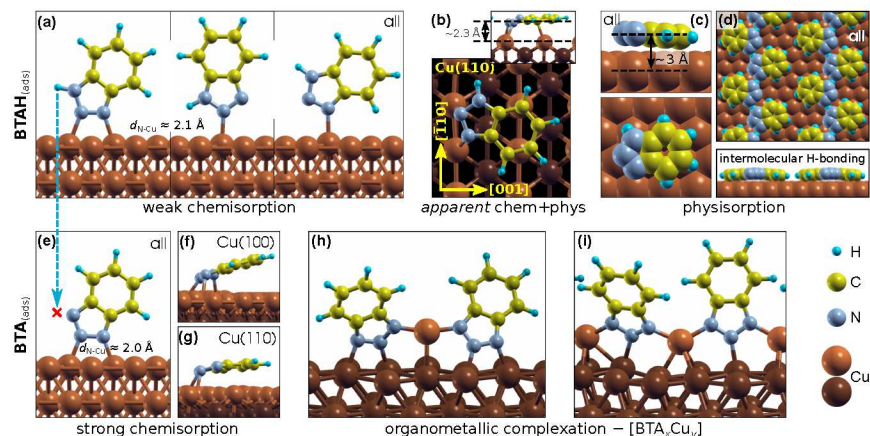
Fig. 1 Various adsorption forms of benzotriazole on copper surfaces identified by means of DFT calculations[5–8,23,25] (label "all" indicates that the form exists on all (several) Cu surfaces). Intact molecular forms (BTAH$_{(ads)}$, top row) and dissociated forms (BTA$_{(ads)}$, bottom row). (a) Weakly chemisorbed modes of BTAH bonded perpendicularly to the surface via triazole nitrogen atoms (d_{N-Cu} stands for N–Cu bond length).[5,6] (b) More strongly bonded parallel adsorption mode of BTAH on Cu(110) that is roughly oriented along the [001] direction; this mode was ascribed as *apparent* chemisorption+physisorption mode (labeled as "*apparent* chem+phys").[6] (c) Physisorption mode with BTAH molecular plane nearly parallel to the surface[6,7] and (d) intermolecular H-bonded networks of physisorbed BTAH;[7] this lateral H-bonding stabilizes the physisorbed BTAH by about 0.5 eV. (e) Strongly chemisorbed BTA$_{(ads)}$ bonded perpendicularly to the surface;[7,8] on Cu(100) and Cu(110) also highly tilted (f) and almost parallel (g) variants were identified.[8] (h,i) Benzotriazole–copper organometallic complexes: (h) [BTA–Cu–BTA] dimer[25] and (i) [BTA–Cu]$_n$ polymer.[7]

tances of about 2.1 Å (Fig. 1a) or physisorb† nearly parallel (BTAH$_∥$) to copper surfaces (Fig. 1c) with the molecule–surface height ranging from about 2.6 Å on Cu(110) to 3 Å on Cu(111).[6] While the adsorption bonding of BTAH$_⊥$ becomes stronger as passing from densely packed Cu(111) to more open surfaces and low coordinated defects, the physisorption energy is similar on all three low Miller index surfaces (Fig. 2);[6] a notable exception for the latter is the so-called *apparent* chemisorption+physisorption mode on Cu(110) (Fig. 1b), which adsorbs significantly stronger (Fig. 2).[6]

3.1.2　Adsorption forms of BTA$_{(ads)}$. In contrast to intact BTAH$_{(ads)}$, dissociated BTA$_{(ads)}$ strongly bonds to copper surfaces and the magnitude of chemisorption energy increases as the coordination number of surface Cu atoms involved in the adsorption site decreases (Fig. 2).[8] Dissociated benzotriazole can also form organometallic complexes on surfaces of copper (Fig. 1h,i); these complexes are specifically addressed in section 3.4.

---

† Terms chemisorption and physisorption refer to the type of molecule–surface interaction and not to the scale of the interaction energy. Molecule–surface bond length is a good descriptor to distinguish between the two. For chemisorption the benzotriazole–surface distances are about 2 Å, whereas for physisorption the distances are about 3 Å as inferred from respective covalent and van der Waals radii.[23]
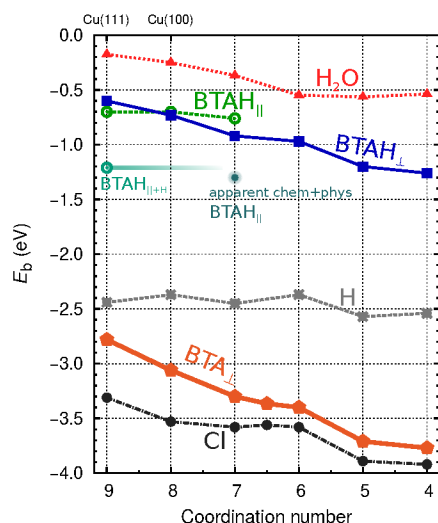
Fig. 2 Dependence of low coverage adsorption (binding) energies of BTAH,[6] BTA, Cl, H,[8] and H_2O-molecule on coordination number of surface Cu atoms at adsorption site (parallel BTAH modes are calculated with the PBE-D' functional, while for all the others the PBE is used). Only the stablest identified adsorption energies at a given coordination number are reported (for BTAH, BTA, Cl, and H see refs. 6,8, whereas for H_2O the points correspond to adsorption on (111), (100), (110), and adtetramer, adtrimer, and addimer defects on Cu(111)).
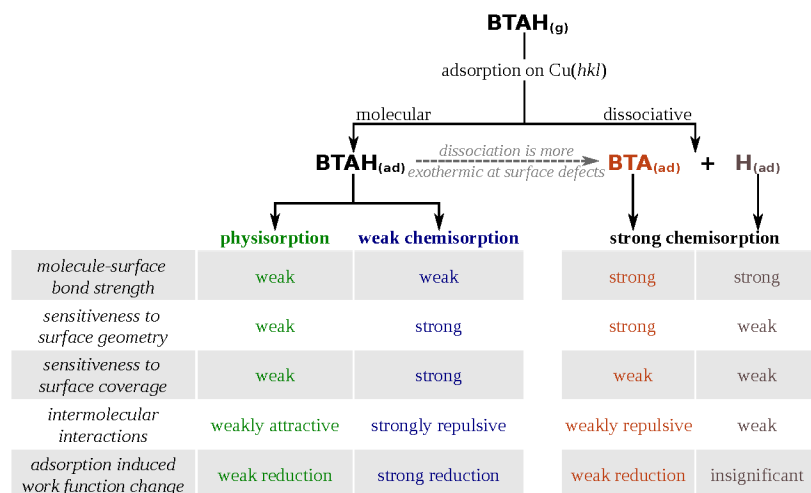
Scheme 2 Characteristics of molecular and dissociative adsorption of benzotriazole on copper surfaces.

3.2 Adsorption characteristics

Adsorption forms of benzotriazole can be classified into four types: (i) weakly chemisorbed $BTAH_{(ads)}$, (ii) physisorbed $BTAH_{(ads)}$ (including the H-bonding networks of Fig. 1d), (iii) standalone strongly chemisorbed $BTA_{(ads)}$, and (iv)
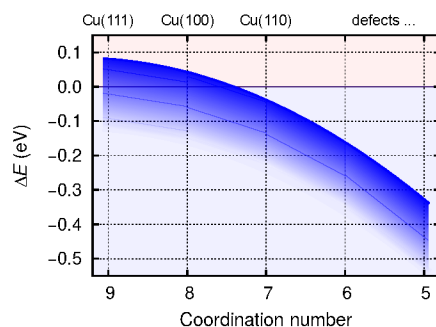
Fig. 3 Schematically shown dependence of benzotriazole dissociation energies ($BTAH_{(ads)} \rightarrow BTA_{(ads)} + H_{ads}$, cleavage of N1–H bond) on coordination number of surface Cu atoms involved in the adsorption site; based on data of ref. 27. Dissociation energy (ΔE) is very sensitive to surface coverage due to a pronounced intermolecular repulsion between adsorbed BTAH (*cf.* Fig. 4). The dependence of ΔE on coverage is roughly indicated by the thickness of the blue band; the larger is the coverage the more exothermic is the ΔE.

BTA–Cu adcomplexes. These four types display rather different adsorption features and for the first three types several adsorption related properties are listed in Scheme 2 (the BTA–Cu adcomplexes are treated separately later) .

3.2.1 Molecule–surface bond strength and role of surface geometry.
Although the intact $BTAH_{(ads)}$ bonds weakly and dissociated $BTA_{(ads)}$ bonds strongly to copper surfaces, the $BTAH_{(ads)} \rightarrow BTA_{(ads)} + H_{(ads)}$ dissociation is slightly endothermic on Cu(111) in the limit of zero coverage. The reason is the cost for the breakage of the N1–H bond; namely, the dissociation energy can be written as:

$$\Delta E_{diss} = E_b^{BTA^{\odot}} + E_b^{H} - E_b^{BTAH} + D_{N1-H}, \tag{2}$$

where $E_b^{BTA^{\odot}}$, E_b^{H}, and E_b^{BTAH} are binding energies of respective species to copper surface; D_{N1-H} is the N1–H bond strength (4.7 eV). For Cu(111) the respective numbers in the limit of zero-coverage are: $\Delta E_{diss} = -2.8 + (-2.4) - (-0.6) + 4.7$ eV $= 0.1$ eV.

In order for dissociation to be exothermic, the following criterion has to be met (*cf.* eqn (2)):

$$E_b^{BTAH} - E_b^{BTA^{\odot}} > E_b^{H} + D_{N1-H}. \tag{3}$$

The bonding of H is rather insensitive to surface details and on Cu(hkl) the $E_b^{H} \in [-2.4, -2.5]$ eV (see Fig. 2). Hence the $BTA_{(ads)}$ has to bond by about 2.3 eV stronger to the surface than $BTAH_{(ads)}$ for dissociation to be exothermic. This criterion is met on open surfaces and low coordinated defects, because the enhancement of the molecule–surface bond strength is larger for $BTA_{(ads)}$ than for $BTAH_{(ads)}$ as the coordination number of surface Cu atoms involved in the adsorption site decreases (see Fig. 2); consequently dissociation energy becomes more exothermic in the same direction (Fig. 3).

In addition to $BTAH_{(ads)}$, $BTA_{(ads)}$, and $H_{(ads)}$, Fig. 2 plots also the dependence of adsorption (binding) energy of $Cl_{(ads)}$ and $H_2O_{(ads)}$ on the coordination number of surface Cu atoms involved in the adsorption site; the former may be
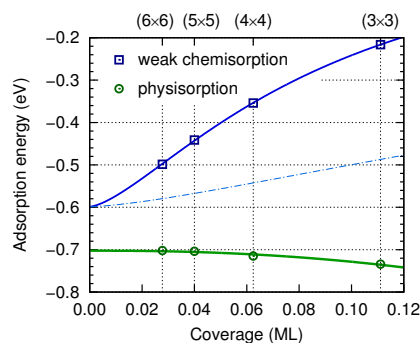
Fig. 4 Dependence of adsorption energy on the coverage for weakly chemisorbed (blue squares) and physisorbed (green circles) BTAH on Cu(111); adsorption energies are taken from ref. 6. The ML unit is defined as the number of molecules per surface Cu atom. Curves and zero-coverage adsorption energies are obtained with a polarizable point-dipole model extrapolation of ref. 32. The dependence is plotted up to a coverage of 0.12 ML, where the physisorbed BTAH$_\parallel$ reaches optimum;[23] at larger coverage the molecules start to feel intermolecular Pauli repulsion. At the water/solid interface the long range lateral intermolecular interactions would be screened by the solvent molecules; the effect is roughly indicated by thin dash-dotted blue line, which approximates the lateral dependence for the permitivitty of $\varepsilon = 6$, which is a typical value for water in the double-layer[33] (note that continuum dielectric approximation is not expected to be valid at short intermolecular distances and also the magnitude of adsorption energy would be significantly altered by solvent effects).

seen as a prototype corrosive species and the latter is relevant due to the importance of water/metal interface for corrosion (though there is a huge difference between a film of liquid water and a single water molecule).

3.2.2 Role of molecular dipole on lateral intermolecular interactions. Among the species considered in Fig. 2, the neutral BTAH displays far the strongest dependence of adsorption energy on surface coverage. This dependence is due to a large permanent dipole moment of BTAH (4.1 D), which results in repulsive and long range dipole–dipole interactions between perpendicularly adsorbed BTAH molecules, while for parallelly physisorbed BTAH the lateral interactions are far less important and slightly attractive at higher coverages (see Fig. 4).[6,32] On the other hand, lateral dipole–dipole interactions are not that important for BTA$_{(ads)}$ due to considerable adsorption induced charge transfer, which greatly reduces the dipole.[7]

Due to the strong lateral intermolecular repulsion between weakly chemisorbed BTAH$_{(ads)}$ and much weaker lateral interactions for BTA$_{(ads)}$ the dissociation of benzotriazole becomes more favorable as the surface coverage increases (this effect is indicated schematically by the width of the blue band in Fig. 3).

3.2.3 Role of molecular dipole on adsorption induced work function change. In addition to long-range lateral intermolecular interactions, a large permanent molecular dipole can also lead to a significant adsorption induced dipole moment (μ), which alters the metal work function by $\Delta\Phi = -4\pi\theta\mu$ (in atomic

Table 1 Adsorption induced dipole moments (μ) and work function changes ($\Delta\Phi$) on Cu(111) due to adsorption of benzotriazole. For comparison, values for $Cl_{(ads)}$, $H_{(ads)}$, and adsorbed H_2O-molecule are also listed.

species	adsorption mode	shown in	coverage (ML)	μ (D)	$\Delta\Phi$ (eV)
$BTAH_\perp$	N2+N3[a]	Fig. 1a	1/9	3.15	−2.25
			1/16	4.72	−1.90
$BTAH_\parallel$	standalone	Fig. 1c	1/9	0.84	−0.62
	H-network	Fig. 1d	1/10	0.96	−0.64
$BTA_{(ads)}$	N2+N3[a]	Fig. 1e	1/16	0.51	−0.21
$[BTA-Cu]_n$	N1+N2+N3[a]	Fig. 1i	2/23	1.91	−1.07
			1/5	1.18	−1.52
$Cl_{(ads)}$	fcc	/	1/9	−0.34	+0.24
$H_{(ads)}$	fcc	/	1/4	−0.03	+0.04
$H_2O_{(ads)}$	top	/	1/9	+0.68	−0.49

[a] Notation indicates which N atoms bond to Cu. The N1 and N3 atoms are symmetry equivalent for BTA.
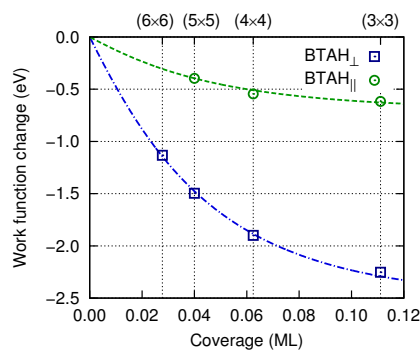

Fig. 5 Dependence of $\Delta\Phi$ of Cu(111) on the coverage of weakly chemisorbed ($BTAH_\perp$, blue squares) and physisorbed ($BTAH_\parallel$, green circles) benzotriazole. The curves are drawn by fitting the data points with polarizable point-dipole model of ref. 32.

units), where θ is the surface coverage (in molecule/bohr^2 unit); positive value of μ stands for an outward-pointing dipole with the negative end at the surface and the positive end pointing outward (*i.e.*, $\mu = \boldsymbol{\mu} \cdot \boldsymbol{n}$, where $\boldsymbol{n}$ is the surface normal and $\boldsymbol{\mu}$ is the dipole of adsorbed molecule). The adsorption induced dipole moment due to a weakly chemisorbed $BTAH_\perp$ is remarkably large (Table 1). Fig. 5 illustrates the dependence of $\Delta\Phi$ of Cu(111) on the coverage of adsorbed BTAH. Even at rather small molecular coverage the reduction of work function is appreciable. Also the $[BTA-Cu]_n$ organometallic complex significantly affects the work function, whereas standalone-$BTA_{(ads)}$, $Cl_{(ads)}$, and $H_{(ads)}$ do not (Table 1). Altered work function affects the adsorption of ions and this issue is discussed in Section 3.3.1.

In this respect it should be noted that large permanent molecular dipole of

inhibitor molecule does not automatically lead to a reduction of work function. It depends on the adsorption structure of inhibitor and for a weakly chemisorbed BTAH on copper, the adsorption structure is such that this is true.
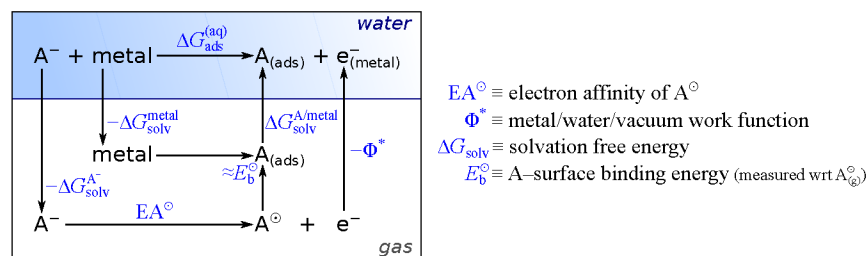
Scheme 3 Thermodynamic cycle used to obtain a rough estimate for the adsorption energy of deprotonated molecule (or anion) in the aqueous phase (mnemonic: A stands for adsorbate or anion).

3.3 Adsorption at water/metal interface

In the above discussion the adsorption of benzotriazole was considered at vacuum/copper interface, but in the context of corrosion inhibition the water/metal interface is more relevant. The presence of aqueous solvent considerably affects the energetics of adsorption due to an interplay of several competitive effects, *i.e.*, molecule–metal, molecule–water, and metal–water interactions. In order to understand these effects, the presence of water has to be either implicitly or explicitly considered in calculations. The explicit modeling is, however, rather tedious. For this reason, the involved effects have been only roughly estimated[7,8] by following an approach that utilizes a thermodynamic cycle,[34] which is shown in Scheme 3. The adsorption energy of deprotonated BTA$^-$ or any other anion from the solution ($A^-_{(solv)} \rightarrow A_{(ads)} + e^-_{(metal)}$) can be written as:[‡]

$$\Delta G^{(aq)}_{ads} \approx (E^\ominus_b - \Delta G^{A^-}_{solv}) + (EA^\ominus - \Phi^*) + \Delta\Delta G^{A//metal}_{solv}, \qquad (4)$$

where:

$$\Delta\Delta G^{A//metal}_{solv} = \Delta G^{A/metal}_{solv} - \Delta G^{metal}_{solv}, \qquad (5)$$

and Φ^* is the work function of the metal/water/vacuum system, which can be written as:

$$\Phi^* = \Phi + \Delta\Phi, \qquad (6)$$

where Φ is the metal work function and $\Delta\Phi$ is its variation due to a thick layer of liquid water.[35] For the meaning of other terms, refer to Scheme 3. The terms were deliberately grouped in parentheses in eqn (4) to illustrate the competitive effects. The first grouped terms represent the competition for the molecule between the metal surface and the solvent. The second grouped terms represent the

---

[‡] Eqn (4) is a straight blend of energy contribution ($E^\ominus_b$) and solvation free energy terms; neither the zero-point energy correction nor the concentration (translational) and roto-vibrational entropy contributions to free energy are taken into account. The equation is therefore very approximate, but it should suffice to illustrate the discussed points.

competition for the electron between the molecule and the metal surface. Each of these four terms is large in magnitude for anions such as BTA$^-$ and Cl$^-$ (*e.g.*, few to several eVs), whereas the last term in eqn (4) is expected to be small in magnitude for copper surfaces (well below the 1 eV).[7,8,36]

For the adsorption of neutral species (A$_{(solv)} \rightarrow$ A$_{(ads)}$) the corresponding eqn is simpler, because there are no electron terms. Hence:

$$\Delta G_{ads}^{(aq)} \approx (E_b - \Delta G_{solv}^A) + \Delta\Delta G_{solv}^{A//metal}. \tag{7}$$

In this case the E_b and ΔG_{solv}^A of BTAH are much smaller in magnitude than the corresponding terms for deprotonated BTA$^-$ (or any other anion).

A large mutual cancellation between the competitive terms in eqns (4) and (7) results in moderate adsorption energies. As a consequence the huge difference between the gas-phase adsorption energies of BTAH$_{(ads)}$ and BTA$_{(ads)}$ is greatly reduced in aqueous-phase. Solvent effects also relatively favor the adsorption of BTA$^-$ compared to Cl$^-$, because Cl$^-$ is much smaller than BTA$^-$ and solvates by about 0.6 eV stronger; Cl also displays by ≈ 0.15 eV larger electron affinity than BTA$^\odot$. While in gas-phase Cl adsorbs stronger than BTA$_{(ads)}$ (see Fig. 2), the two just mentioned effects seem to reverse the adsorption energy trend and BTA$_{(ads)}$ *wins* over Cl$_{(ads)}$ in aqueous-phase.[8]

Solvent effects also diminish the adsorption energy dependence on the co-ordination of surface metal atoms, because the adsorbate has to displace water molecule(s) from the surface during specific adsorption and water displays similar bonding enhancement trend as benzotriazole and Cl$_{(ads)}$ (Fig. 2). This effect is captured by the $\Delta\Delta G_{solv}^{A//metal}$ term in eqns (4) and (7). For anionic species (BTA$^-$ and Cl$^-$) there is an additional effect that is even more pronounced and is due to dependence of Φ^* on the surface geometry. Namely, the reduction of Φ^* as going from (111) to (110) is so large§ that it reverses the adsorption trend, *i.e.*, estimated magnitudes of aqueous-phase adsorption energies of BTA$^-$ and Cl$^-$ follow the $(111) \gtrsim (100) > (110)$ sequence.[8] This finding is in agreement with the analysis of electrochemical experiments of Trasatti *et al.*,[38,39] who reported the same crystal-face specificity trend for the adsorption of halide anions on Ag.

3.3.1 Role of inhibitor induced work function change. Weakly chemi-sorbed BTAH considerably reduces the work function (Table 1). Such a pronounced effect on the work function should, according to eqn (4), drastically affect the adsorption of anions. On this basis one can argue that reduced work function should *diminish* any reaction that donates electron(s) to the metal, such as the adsorption of corrosive chloride anions (Cl$^-_{(solv)} \rightarrow$ Cl$_{(ads)}$ + e$^-_{(metal)}$), dissolution of metal (*e.g.*, Cu$_{(solid)} \rightarrow$ Cu$^{n+}_{(solv)}$ + ne$^-_{(metal)}$), or oxidation of metal (*e.g.*, $2 Cu + H_2O \rightarrow Cu_2O + 2 H^+ + 2 e^-$).

By comparing Figs. 4 and 5, it can be seen that the effect of molecular dipole on the work function is larger than on the adsorption energy. The effect of molecular dipole on the inhibitor–surface bonding has been often discussed in studies

---

§ Both Φ and $\Delta\Phi$ (*cf.* eqn (6)) reduce with reducing the coordination of surface Cu atoms; the PBE calculated Φ values are 4.84, 4.60, and 4.39 eV for Cu(111), Cu(100), and Cu(110), respectively,[37] while the experimentally estimated $\Delta\Phi$ at potential of zero charge are -0.54, -0.57, and -0.65 eV, respectively,[38] which result in Φ^* values of 4.29, 4.03, and 3.74 eV for (111), (100), and (110) faces, respectively.[8]

that correlate inhibitor electronic parameters with their inhibition efficiency, but the effect on the work function has not been appreciated.
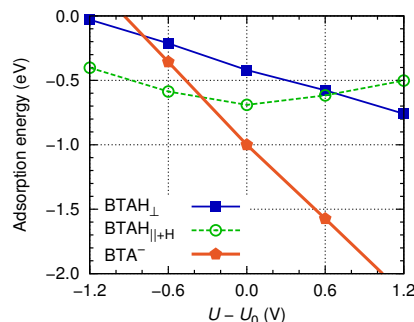

Fig. 6 Roughly estimated dependence of adsorption energy of benzotriazole on copper surfaces (*i.e.*, values are averaged as $\approx \frac{1}{3}$[Cu(111) + Cu(100) + Cu(110)]) on the electrode potential relative to *static* potential of zero charge, U_0.¶ The following species are considered: weakly chemisorbed BTAH (labeled as $\text{BTAH}_\perp$, structure shown in Fig. 1a), physisorbed BTAH intermolecularly associated into a H-bonded network ($\text{BTAH}_{\parallel+\text{H}}$, Fig. 1d), and deprotonated BTA^- (Fig. 1e).

3.3.2   Electric field effects in the double-layer. The electric field ($\boldsymbol{E}$) in the double-layer influences the adsorption due to several effects, which according to the current model can be decomposed into: (i) variation of the molecule–surface bonding, (ii) variation of contribution due to electron transfer from anion to electrode (or to cation from electrode), and (iii) variation of the $\Delta\Delta G_{\text{solv}}^{\text{A//metal}}$ term. These effects were roughly estimated in Ref. 7¶ and here this method is utilized to discuss the effect of electrode potential on various adsorbed forms of benzotriazole. In particular, Fig. 6 plots the estimated dependence of the aqueous-phase adsorption energy on the electrode potential for the weakly chemisorbed

---

¶The effects (i) and (ii) were estimated by putting the slab model (either adsorbate/copper or water-film/copper) in homogeneous electric field $\boldsymbol{E}$ and performing relaxation calculations at several different values of electric field. The relation between the electric field and electrode potential (U) was treated within the Helmholtz-Perrin parallel plate capacitor model of double layer, *i.e.*:

$$U = U_0 + d\boldsymbol{n} \cdot \boldsymbol{E}, \tag{8}$$

where U_0 is the electrode potential corresponding to $\boldsymbol{E} = 0$, which can be seen as a *static* potential of zero charge (spzc), but notice that spzc can be different from the measurable potential of zero charge. [40] The proportionality constant d is the thickness of a double layer, which was approximated by the often used value of $d = 3$ Å. [41–43] The adsorption energies were then calculated as:

$$\Delta G_{\text{ads}}^{(\text{aq})}(\boldsymbol{E}) = \Delta G_{\text{ads}}^{(\text{aq})}(0) + \delta E_{\text{b}}^{\odot}(\boldsymbol{E}) + \delta\Delta\Delta G_{\text{solv}}^{\text{A//metal}}(\boldsymbol{E}) + ze(U - U_0), \tag{9}$$

and

$$\delta E_{\text{b}}^{\odot}(\boldsymbol{E}) = E_{\text{b}}^{\odot}(\boldsymbol{E}) - E_{\text{b}}^{\odot}(0),$$

$$\delta\Delta\Delta G_{\text{solv}}^{\text{A//metal}}(\boldsymbol{E}) = \Delta\Delta G_{\text{solv}}^{\text{A//metal}}(\boldsymbol{E}) - \Delta\Delta G_{\text{solv}}^{\text{A//metal}}(0),$$

where e is the unit charge and z is the charge of the species in solution (-1 for BTA^- and 0 for BTAH). For more details see the Supporting Information of Ref. 7.


This journal is © The Royal Society of Chemistry [year]

BTAH (labeled as $BTAH_\perp$), physisorbed BTAH intermoleculalry associated into H-bonding network ($BTAH_{\parallel+H}$), and deprotonated BTA^-.

This figure should be understood only qualitatively, because the presented adsorption energies are subjected to significant uncertainty due to the nature of involved approximations. Nevertheless, the qualitative trends (*i.e.*, the slopes/shapes of the curves) should be correctly captured. There are few things to notice from the figure: (i) $BTAH_{\parallel+H}$ displays the well known *parabolic* dependence of simple organic moleculars, with the strongest adsorption at the potential of zero charge,[33] whereas (ii) the adsorption energy of $BTAH_\perp$ becomes more exothermic as the electrode potential becomes more positive (almost linearly). This distinctive behavior can be attributed to the orientation of molecular dipole of the two forms, because the variation of molecule–surface bond with electric field is roughly proportional to $-\boldsymbol{\mu}\cdot\boldsymbol{E}$; for physisorbed BTAH the dipole points largely parallel to the surface, hence $-\boldsymbol{\mu}\cdot\boldsymbol{E}\approx 0$ and the parabolic dependence stems from the enhancement of water–metal interaction with increasing $\boldsymbol{E}$. On the other hand, the dipole of $BTAH_\perp$ points outward and in this case $\partial E_b/\partial U \approx \mu/d = 0.3$ e (if $d = 3$ Å and μ is taken from Table 1).$^{\parallel}$ (iii) Finally, the slope of BTA^- line is largely dominated by the $-e(U - U_0)$ term, eqn (9), and is thus close to one.

According to Fig. 6, the $BTAH_{\parallel+H}$ form is the stablest among the three forms at low values of potential ($U - U_0 \lesssim -0.3$ V), but at larger values deprotonated form becomes the stablest. The curves in Fig. 6 correspond to the following reactions:

$$BTAH_{(solv)} \rightarrow BTAH_{(ads)} \qquad \text{and} \qquad (10)$$

$$BTA^-_{(solv)} \rightarrow BTA_{(ads)} + e^-_{(metal)}, \qquad (11)$$
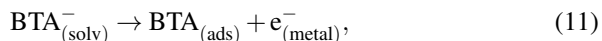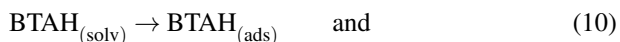
which implies that $BTAH_{(ads)}$ and $BTA_{(ads)}$ are treated as independent. This may not always be the case due to a dissociation reaction at the surface:

$$BTAH_{(ads)} \rightleftharpoons BTA_{(ads)} + H_{(ads)}. \qquad (12)$$
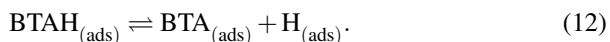
Alternatively the H1a proton can be abstracted by a neighboring water molecule (which may then diffuse away from the surface):

$$BTAH_{(ads)} \rightleftharpoons BTA_{(ads)} + H^+ + e^-. \qquad (13)$$
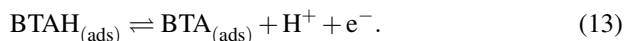
The argument applies to both cases. Consider, for example, the desorption of $BTA_{(ads)}$ under low pH conditions.** If the barrier for the reverse of reaction (12) or (13) is not too large, it may be more convenient for $BTA_{(ads)}$ to desorb as $BTAH_{(ads)}$; namely, the larger is the coverage of $H_{(ads)}$ (or concentration of H^+)

$^{\parallel}$ This implies that E_b changes by ≈ 0.3 eV if potential is altered by 1 V. The actual calculations reveal that the variation is even larger due to molecular polarization, but this extra effect is largely canceled by the enhancement of the water–metal interaction with increasing $\boldsymbol{E}$ (note that water has a considerably smaller dipole moment than BTAH); hence the slope of $BTAH_\perp$ line in Fig. 6 is close to 0.3 e.

** Although the argument is similar for both reactions, (12) and (13), the atomistic mechanism is different. In the reverse direction of reaction (12) $BTA_{(ads)}$ reacts with $H_{(ads)}$ (Langmuir–Hinshelwood mechanism), while in the reverse of reaction (13) the H^+ comes from solution and reacts with $BTA_{(ads)}$ directly (Eley–Rideal mechanism).

---

the more to the left the reaction (12) (or (13)) is pushed. This argument, together with Fig. 6, suggests that $BTA_{(ads)}$ is more relevant at higher potentials and higher pH, while $BTAH_{(ads)}$ may dominate at low potentials and low pH (relatively speaking); this is in fact self-evident from reaction (13). With respect to corrosion inhibition, it would be desirable to make reaction (12) *irreversible* or at least to push the dissociation reaction to the right as much as possible, because $BTA_{(ads)}$ bonds much stronger to the surface than $BTAH_{(ads)}$ and strong bonds imply larger desorption barriers than weak bonds. This may be the case on low coordinated surface defects, because Fig. 3 reveals that dissociation is more exothermic there. A step further in this direction is achieved by the BTA–Cu organometallic complexation, which is an issue that we turn to now.

3.4 Role of BTA–Cu organometallic complexes

The ability of benzotriazole to inhibit corrosion was often attributed to formation of protective BTA–Cu surface complexes.[††] The arguments presented above may provide a sound rationale of why this is so. According to DFT calculations,[7,8] the BTA–Cu organometallic complexes are thermodynamically more stable than standalone chemisorbed $BTA_{(ads)}$. For example, the two organometallic complexes—shown in Fig. 1h,i—are by about 0.1 to 0.2 eV/BTA more stable than the standalone form. This difference is not large, but it includes the cost for the Cu adatoms formation (0.76 eV/atom on Cu(111)) that are incorporated into the complex (for more details, see Ref. 8). This implies that the gross bonding of BTA within the organometallic complex is much stronger than the BTA–surface bond of standalone form. Moreover, within the complex all the BTA's N atoms are bonded to Cu atoms and are thus saturated (*cf.* Fig. 1h,i). Hence, the removal of BTA or the fusion of H into the BTA are more unlikely for the complex than for the standalone form. The organometallic complexes are therefore more resistant than the standalone $BTA_{(ads)}$ forms to the reverse of reaction (12) or (13), which eventually leads to desorption of benzotriazole. But they are still susceptible to potential and pH, according to the reaction of Youda:[47] $nBTAH_{(ads)} + nCu \rightleftharpoons [Cu–BTA]_n + nH^+ + ne^-$.

According to some researchers the formation of protective BTA–Cu complex is faster on bare metallic surfaces[16], while others emphasized the importance of surface oxides in their formation.[14,46] The latter is one among reasons that the adsorption of benzotriazole on oxidized copper surfaces is considered below.

4   Adsorption of benzotriazole on oxidized copper surfaces

Up to this point the bonding of benzotriazole with reduced (oxide-free) copper surfaces was considered, which are more relevant at acidic pH, but in other conditions the copper surfaces are oxidized. It should be noted that bare metallic surfaces are structurally and electronically simpler than oxidized surfaces, which is

---

†† Linear polymeric structure consisting of alternating Cu^+ and BTA^- ions in 1:1 ratio that form a –Cu–BTA–Cu–BTA– bidentate structure was usually proposed;[9,10,44–46] a corresponding model of such $[BTA–Cu]_n$ adstructure on bare copper surface, as obtained by DFT calculations, is shown in (Fig. 1i).[7] Recently, Chen and Häkkinen proposed, on the basis of DFT calculations, a [BTA–Cu–BTA] dimer adstructure (Fig. 1h).[25] This adcomplex was recently observed experimentally by STM (scanning tunneling microscopy) under ultra-high-vacuum conditions on Cu(111).[28,31]

the reason that the bonding of benzotriazole to oxidized copper surfaces has been considered by DFT calculations to a sufficiently smaller extent than to bare copper surfaces. Jiang and Adams[48] studied the bonding of BTAH on stoichiometric $Cu_2O(111)$, while Peljhan and Kokalj[49,50] extended the calculations and considered also the bonding on thermodynamically stablest so-called $Cu_2O(111)$-w/o-Cu^{CUS} and $Cu_2O(110):CuO$. Currently, the adsorption of benzotriazole is considered in more detail on a broader set of potential surface sites on oxidized copper surfaces.

Because oxidized surfaces may display a plethora of different structures and stoichiometries, some of which might be rather complicated, a reductionistic approach is followed The surfaces of Cu_2O are well characterized in gas-phase and these are taken as a starting model of oxidized copper surface (section 4.1). Subsequently also simple models of hydroxylated Cu_2O surface are considered (section 4.2), because several studies indicate that surface oxide layer is likely hydroxylated in aqueous solution.[51–54] Due to obvious modeling reasons, the reported results again refer to the solid/vacuum interface and all the models are based on cuprous oxide (the Cu(II) oxidation state is not considered). In this respect it should be noted that the Cu_2O is more relevant than CuO for the formation of protective film of benzotriazole.[13]

4.1 Cu_2O as a model of oxidized copper surfaces

4.1.1 Stability of various Cu_2O surfaces. The stability of various Cu_2O surfaces in ambient of oxygen atmosphere was characterized in detail by Soon *et al.* by means of DFT calculations.[55,56] Two surfaces display notably lower surface free energies than the others; one of them is the $Cu_2O(111)$-w/o-Cu^{CUS} (Fig. 7c). It differs from stoichiometric $Cu_2O(111)$ (Fig. 7a,b) by the absence of coordinately unsaturated (CUS) copper atoms; the label "$Cu_2O(111)$-w/o-Cu^{CUS}" thus stands for $Cu_2O(111)$ without Cu CUS atoms. The STM study of Önsten *et al.*[57] seems to have identified the $Cu_2O(111)$-w/o-Cu^{CUS} structure (their proposed model B). According to their nomenclature this surface was labeled as (1×1). In addition, they also observed the $(\sqrt{3} \times \sqrt{3})R30°$ reconstructed surface, where one third of surface oxygens (O^{up} as defined in Fig. 7) are missing. A characteristic of the $(\sqrt{3} \times \sqrt{3})R30°$ is the presence of the $Cu^{O_{vac}}$ sites that are described below. Under electrochemical conditions the $Cu_2O(111)$ surface can be Cu terminated (labeled as $Cu_2O(111):Cu$) and stabilized by adsorbed hydroxyls.[51,52,58] Adsorption of benzotriazole on hydroxylated $Cu_2O(111)$ is considered in section 4.2.

4.1.2 Description of considered adsorption sites. Fig. 7 shows the structure of stoichiometric $Cu_2O(111)$, $Cu_2O(111)$-w/o-Cu^{CUS}, and Cu terminated $Cu_2O(111):Cu$. It also defines the naming of various atoms (ions) in the near surface region. Some atoms (ions) in the surface region are coordinatively saturated (CSA) and others are coordinatively unsaturated (CUS); caption of Fig. 7 explicitly lists all the CSA and CUS atoms. Note that the naming of atoms does not follow the coordinative CSA/CUS description (only the surface Cu atoms of stoichiometric $Cu_2O(111)$ are named Cu^{CUS} and Cu^{CSA}), but rather more structural-like description, *e.g.*, O^{up} and O^{dn} indicate that they are above and below the surface Cu layer, respectively. The Cu atoms, which surrounds the O^{up}
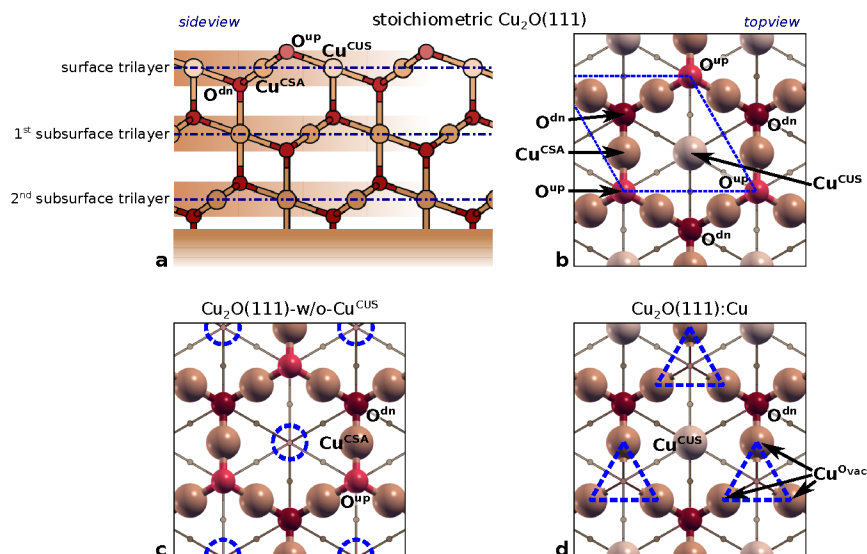
Fig. 7 Structures of various considered Cu_2O surfaces (copper and oxygen atoms are colored brownish and reddish, respectively). For clarity of presentation non-relaxed (non-reconstructed) structures are plotted and surface trilayers are *emphasized* in the top-view plots. (a,b) Side- and top-view of stoichiometric $Cu_2O(111)$; note the stacking of O–Cu–O trilayers shown in the sideview. There are six atoms in the surface trilayer per (1×1)–unit cell (indicated by blue dashed parallelogram in (b)): $3 \times Cu^{CSA}$, $1 \times Cu^{CUS}$, $1 \times O^{up}$, and $1 \times O^{dn}$ (note that O^{dn} is CSA and O^{up} is CUS). (c) Non-stoichiometric $Cu_2O(111)$ without Cu^{CUS} atoms (labeled as $Cu_2O(111)$-w/o-Cu^{CUS}); Cu^{CUS} vacancies are indicated by blue dashed circles. (d) Cu terminated $Cu_2O(111)$ surface (labeled as $Cu_2O(111)$:Cu), which can be seen as stoichiometric $Cu_2O(111)$ without O^{up} atoms; O^{up} vacancies are indicated by blue dashed triangles and the surrounding Cu atoms are labeled as Cu^{Ovac} (note that Cu^{Ovac} is CUS).

vacancy (Fig. 7d) are CUS, but they are named Cu^{Ovac} as to differentiate them from Cu^{CUS} of stoichiometric $Cu_2O(111)$).

Calculations on $Cu_2O(111)$ surfaces were performed with slabs that consist of four trilayers. A (2×2) supercell was used. Its size would correspond to $Cu(111)$–(4×4), but the lattice parameter of Cu_2O bulk (4.35 Å, PBE value) is larger than for Cu (3.67 Å), hence it actually corresponds to the size of $Cu(111)$–(4.7×4.7) supercell. Because of the coverage dependence of BTAH adsorption energies (*cf.* Fig. 4), this should be kept in mind when comparing the results between oxidized an reduced copper surfaces. The $Cu_2O(111)$-w/o-Cu^{CUS} was taken as a reference; the adsorption on the Cu^{CUS} and Cu^{Ovac} sites may be hence considered as adsorption on defect sites of $Cu_2O(111)$-w/o-Cu^{CUS}. Two models—one based on $Cu_2O(111)$-w/o-Cu^{CUS} and the other on $Cu_2O(111)$:Cu[‡‡]—were used for each defect as to have an estimate of how sus-

---

[‡‡] The adsorption on Cu^{CUS} and Cu^{Ovac} sites of $Cu_2O(111)$-w/o-Cu^{CUS} model was modeled by adding one Cu^{CUS} and removing one O^{up} ion per (2×2) supercell, whereas $Cu_2O(111)$:Cu model already consists of both Cu^{CUS} and Cu^{Ovac} sites. Note, however, that $Cu_2O(111)$:Cu is a polar terminated surface of Tasker type-3,[59] hence it undergoes a reconstruction.[52] In particular, the O^{dn} ions upshift to the plane of surface Cu ions, the three Cu^{Ovac} ions (marked by blue dashed triangle in Fig. 7d) move
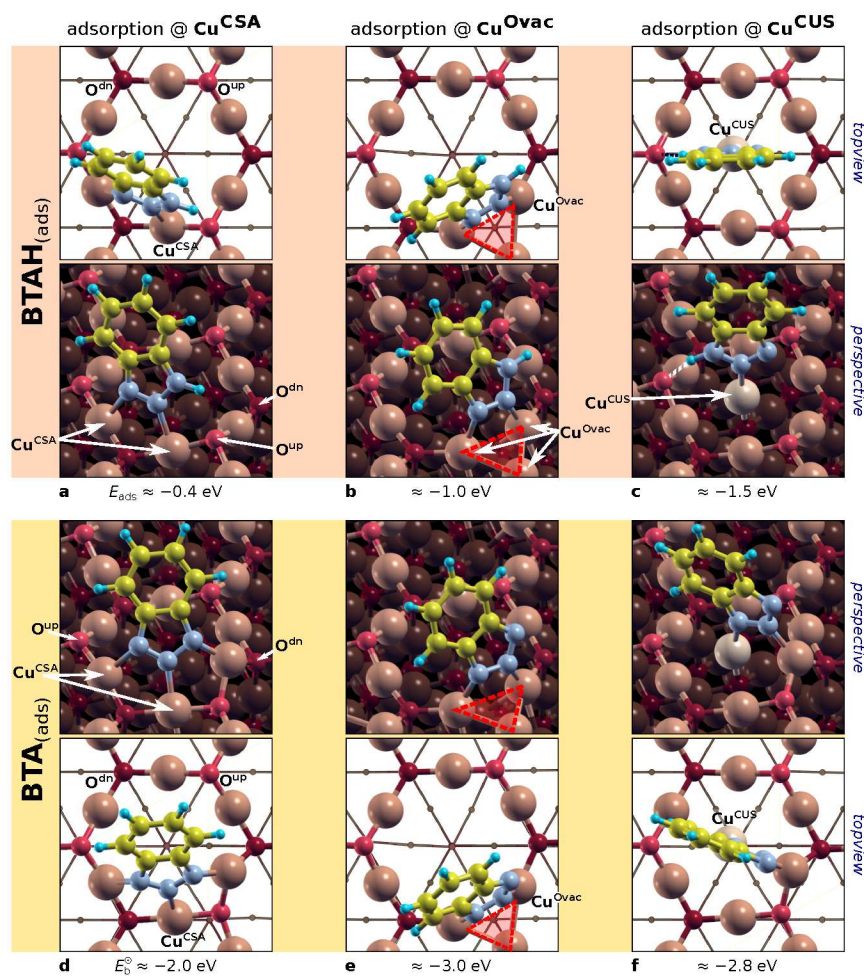
Fig. 8 Top-view and perspective plots of representative structures of $BTAH_{(ads)}$ (top) and $BTA_{(ads)}$ (bottom) on various considered sites of $Cu_2O(111)$; partially based on refs. 49,50. Adsorption (binding) energies are also reported. From left to right: molecular bonding to Cu^{CSA}, $Cu^{O_{vac}}$, and Cu^{CUS} sites. The O^{up} vacancy with the surrounding $Cu^{O_{vac}}$ atoms is indicated by reddish triangle. Note that in addition to direct N–Cu bonds, the BTAH adsorbed at Cu^{CUS} also forms the N1–H···O^{up} hydrogen bond.

ceptible are adsorption characteristics on the specifics of given model (the results

closer to one another and the Cu^{CUS} relaxes laterally as to bond with $Cu^{O_{vac}}$. There are multiple ways of how this can happen and different reconstruction patterns display significantly different stability. For this reason the adsorption of benzotriazole on $Cu_2O(111)$:Cu is modeled using the following recipe: (i) the structure of $Cu_2O(111)$:Cu is optimized, (ii) benzotriazole is added to the structure-(i) and relaxation is performed, and (iii) benzotriazole is removed and the surface is reoptimized. The adsorption energy is then calculated by using the total energies of (ii) and (iii). The reason for step (iii) is that step (ii) lowers the symmetry of the system (*i.e.*, the molecule perturbs the system) and the surface may find new relaxation pattern with lower energy; step (iii) therefore assures that structures (ii) and (iii) have compatible relaxation pattern. A more sophisticated (but computationally way more expensive) approach would be to use simulated annealing technique as was done by Islam *et al.*[52]

were however not too different between different models). The results for adsorption of BTAH$_{(ads)}$ and BTA$_{(ads)}$ on various sites of Cu$_2$O(111) are presented in Figs. 8.

4.1.3 Bonding of BTAH to various sites of Cu$_2$O(111). Optimized adsorption structures of BTAH$_{(ads)}$ are show in Figs. 8a–c. The trend of the molecule–surface bonding follows the order: Cu^{CSA} < Cu$^{O_{vac}}$ < Cu^{CUS}. According to Fig. 8a, the bonding of BTAH to Cu^{CSA} is thus similar to that of Cu(111) (keep in mind that compatible coverages have to be compared), whereas on coordinatively unsaturated Cu$^{O_{vac}}$ and Cu^{CUS} the bonding is considerably enhanced and it is even stronger than on low coordinated defects on bare Cu surfaces (*cf.* Fig. 2). Indeed, the bonding to Cu^{CUS} is so large that it overcompensates the thermodynamic deficiency of Cu^{CUS} and, consequently, the BTAH@Cu^{CUS} is thermodynamically more stable than BTAH@Cu^{CSA}.[†]

4.1.4 Bonding of BTA to various sites of Cu$_2$O(111). Adsorption structures of BTA$_{(ads)}$ are show in Figs. 8d–f. It is evident that also on Cu$_2$O surfaces the BTA$_{(ads)}$ bonds considerably stronger than BTAH$_{(ads)}$, but the difference is smaller than on bare Cu surfaces. The bonding is the weakest on Cu^{CSA} sites, -2.0 eV, while on Cu$^{O_{vac}}$ and Cu^{CUS} sites it is enhanced to -3.0 and -2.8 eV, respectively.

4.1.5 Dissociation of BTAH on various sites of Cu$_2$O. According to eqn (3), the BTA$_{(ads)}$ has to bond by about 2.3 eV stronger to bare Cu surfaces than BTAH$_{(ads)}$ in order for the dissociation to be exothermic. On Cu$_2$O surfaces this difference is smaller (1.7 eV), because H binds stronger to Cu$_2$O (-3.0 eV) than to Cu surfaces.[‡] Nevertheless, the $E_b^{BTAH} - E_b^{BTA^\ominus} > 1.7$ eV condition is met only on Cu$^{O_{vac}}$ sites, which implies that dissociation of BTA$_{(ads)}$ is thermodynamically favored only thereon (the issue is confirmed by separate BTA$_{(ads)}$ + H$_{(ads)}$ coadsorption calculations). It should be noted, however, that under non-acidic conditions, the BTA$^-$ can be also supplied from solution; the BTAH's pKa constant at 25 C$^\circ$ is 8.4 for BTAH$\rightleftharpoons$BTA$^-$ + H$^+$,[60] hence at pH = 7 the BTA$^-_{(solv)}$/BTAH$_{(solv)}$ ratio is 4/96.

4.1.6 BTA–Cu organometallic complexes on Cu$_2$O. The rationale behind the formation of BTA–Cu organometallic complexes on bare Cu surfaces is the stronger bonding of BTA$_{(ads)}$ to low coordinated Cu sites.[8] It was shown above that benzotriazole binds stronger also to coordinatively unsaturated sites on Cu$_2$O surfaces. For this reason the issue of BTA–Cu complexation on oxidized copper surfaces is considered from DFT perspective. The aim is not to identify structures

---

[†] The BTAH bonding enhancement as passing from Cu^{CSA} to Cu^{CUS} is 1.1 eV, while the cost for the Cu^{CUS} formation is between 0.43 and 1.06 eV, taking into account the range of Cu chemical potential between that of Cu and Cu$_2$O bulk, *i.e.*, $\mu_{Cu}^{max} = E_{Cu}^{bulk}$ and $\mu_{Cu}^{min} = \frac{1}{2}[E_{Cu_2O}^{bulk} - \frac{1}{2}E_{O_2}]$, where E_{Cu}^{bulk}, $E_{Cu_2O}^{bulk}$, and E_{O_2} are DFT total energies of Cu atom in the Cu-bulk, formula unit of Cu$_2$O bulk, and oxygen molecule, respectively.

[‡] Note that on Cu$_2$O surfaces, H binds stronger to O than to Cu ion, hence the dissociation reaction should be correspondingly written as:

$$BTAH_{(ads)} + O_{(Cu_2O)} \rightarrow BTA_{(ads)} + OH_{(ads)}, \qquad (14)$$
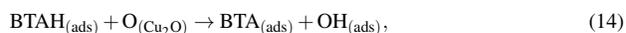
where O$_{(Cu_2O)}$ is the O of the Cu$_2$O surface.

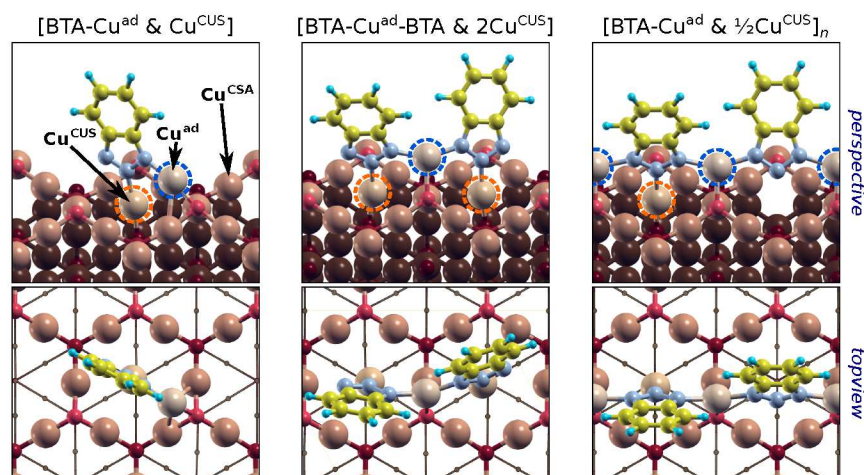**Fig. 9** Various BTA–Cu organometallic complexes on $Cu_2O(111)$-w/o-Cu^{CUS} (perspective and top-view). From left to right: [BTA–Cu^{ad} & Cu^{CUS}] monomer, [BTA–Cu^{ad}–BTA & $2Cu^{CUS}$] dimer, and [BTA–Cu^{ad} & $\frac{1}{2}Cu^{CUS}$]$_n$ polymer. Cu^{ad} stands for Cu adatom that is located above the surface and is incorporated into the complex. Note that, in addition to Cu^{ad}, complexes also involve the Cu^{CUS} atom(s). The naming of complexes reveals the stoichiometry between BTA, Cu^{ad}, and Cu^{CUS}. The Cu^{ad} and Cu^{CUS} are highlighted by dashed blue and orange circles, respectively.

that actually exist—this seems insurmountable without any experimental input— but rather to investigate whether organometallic complexes of benzotriazole are favored over standalone $BTA_{(ads)}$ on oxidized copper surfaces, which is affirmative according to experiments.[13,14,46,61] Several complexes were identified that are more stable than standalone adsorbed $BTA_{(ads)}$ forms, and Fig. 9 shows exemplar monomer, dimer, and polymer adcomplex structures. Gross binding of BTA within the monomer, dimer, and polymer complexes is calculated to be -4.3, -3.8, and -3.7 eV/BTA, respectively. If the cost for the formation of Cu^{CUS} and Cu^{ad} atoms is taken into account (Cu^{ad} stands for Cu adatom), then the formation energies are in range of $[-2.7, -1.4]$, $[-2.7, -1.8]$, and $[-2.6, -1.7]$ eV/BTA for monomer, dimer, and polymer complex, respectively, where the lower number corresponds to μ_{Cu}^{max} and the upper number to μ_{Cu}^{min} (chemical potentials μ_{Cu}^{max} and μ_{Cu}^{min} are defined in the footnote of section 4.1.3). For comparison, the formation energy of $BTA_{(ads)}$ bonded to Cu^{CUS} is in range of $[-2.4, -1.7]$ eV.

4.2 Hydroxylated $Cu_2O(111)$ surfaces

According to current calculations the OH bonds by about 1.9 eV to Cu^{CSA}, 3 eV to Cu^{CUS}, and 3.6 eV to $Cu^{O_{vac}}$ (with respect to OH radical in the gas-phase). Bonding enhancement is thus considerable—a trend similar as for $BTA_{(ads)}$(*cf.* section 4.1.4). This enhancement helps to understand why, in contrast to gas-phase ambient, at water/solid interface the Cu_2O surface can contain appreciable amount of coordinatively unsaturated Cu ions, which are stabilized by adsorbates such as hydroxyls[52] or inhibitor molecules (if present).

Two simple models of hydroxylated surface of Cu_2O were used, one derived
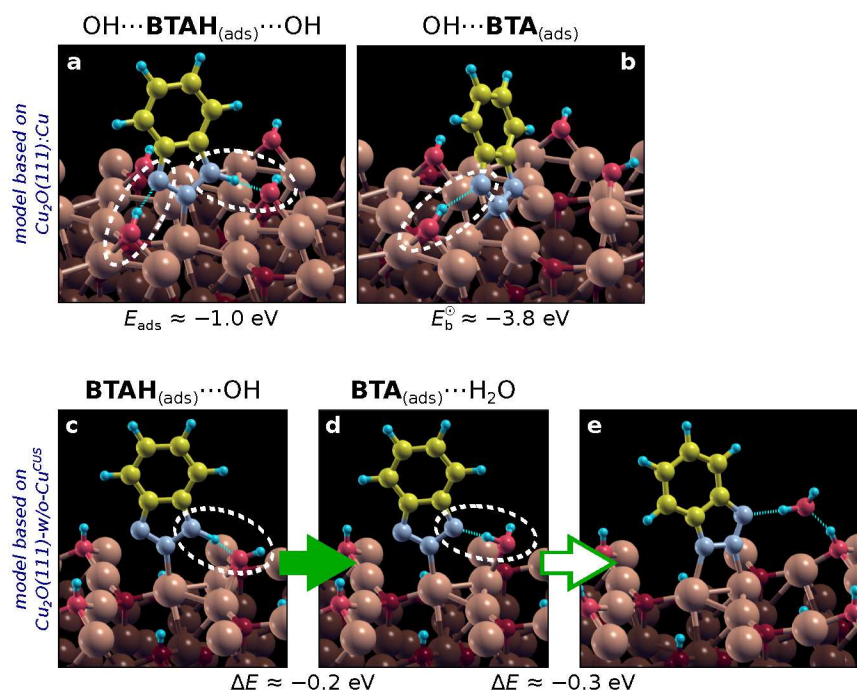
Fig. 10 Adsorption structures of BTAH$_{(ads)}$ and BTA$_{(ads)}$ on two different models of hydroxylated Cu$_2$O(111) surface (refer to the text). The adsorption (binding) energies are also reported in (a,b). Note that in addition to direct N–Cu bonding, benzotriazole also forms hydrogen-bonds with adsorbed hydroxyls (*i.e.*, OH$\cdots$N and/or NH$\cdots$OH bonds), which are indicated by white dashed ellipses. (c,d) Dissociation of adsorbed BTAH by the proton transfer from its N1 atom to OH$_{(ads)}$; the corresponding process is exothermic by 0.2 eV. (e) The BTA$_{(ads)}\cdots$H$_2$O$_{(ads)}$ can further stabilize by 0.3 eV by forming another N–Cu bond and H$_2$O$\cdots$OH hydrogen bond (but the H$_2$O$\cdots$Cu bond is lost).

from Cu$_2$O(111)-w/o-Cu^{CUS} and the other from Cu$_2$O(111):Cu.§ The first can be seen as a model of hydroxylated surface without (or insignificant amount of) unsaturated Cu ions and the second as a model with considerable amount of unsaturated Cu ions. Both models give rather similar benzotriazole–surface binding energies, which are about -1.0 eV for BTAH$_{(ads)}$ (a value similar to the one obtained on Cu$^{O_{vac}}$ sites of plain Cu$_2$O(111) surface) and about -3.8 eV for BTA$_{(ads)}$ (Fig. 10a,b). BTA$_{(ads)}$ thus binds considerably stronger to hydroxylated surface than to plain Cu$_2$O. Consequently, the dissociation of benzotriazole is favored on hydroxylated surfaces. Calculations further reveal that benzotriazole forms hydrogen bonds with the OH$_{(ads)}$ more efficiently than with the O^{up} ions of plain Cu$_2$O. The reason is that hydroxyls are much more flexible than O ions and can easily adjust so as to form hydrogen bonds with benzotriazole's N atoms (see Fig. 10). The flexibility of OH groups also leads to a new dissociation

§ The Cu$_2$O(111)-w/o-Cu^{CUS} derived model was made hydroxylated by substituting all O^{up} and all O ions below the Cu^{CUS} vacancies with OH groups; the model contains 8 hydroxyls per (2×2) supercell. For the Cu$_2$O(111):Cu the model as used by Asthagiri *et al.*[58] was used, where Cu$_2$O(111):Cu– (2×2) supercell contains 4 hydroxyls, which bridge the Cu^{CUS} and Cu$^{O_{vac}}$ atoms.

mechanism of benzotriazole. Namely, in addition to dissociation reaction (14), benzotriazole can dissociate also by interacting with the hydroxyl and forming a water molecule in the course of dissociation:

$$BTAH_{(ads)} + OH_{(ads)} \rightarrow BTA_{(ads)} + H_2O. \qquad (15)$$
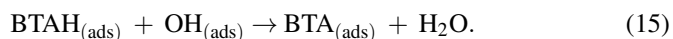
A snapshot of this reaction is shown in Fig. 10c,d. The corresponding elementary dissociative step is exothermic by 0.2 eV, but notice that the resulting $BTA_{(ads)}$ structure (Fig. 10d) is not the stablest possible; the $BTA_{(ads)}$ then further stabilizes by 0.3 eV by forming another N–Cu bond. Water formation has been proposed to form during BTAH dissociation in the literature, although due to interaction with oxygen.[16,62]

5 Conclusions

Controversial suggestions exist in the literature, concerning the role of copper oxides for the adsorption of benzotriazole.[11] To shed some new light onto this question, the adsorption behavior of benzotriazole on reduced and oxidized copper surfaces was discussed on the basis of DFT results. DFT calculations reveal that benzotriazole is able to bond with oxide-free and oxidized copper surfaces. Its bonding is considerably enhanced as passing from Cu(111) to low coordinated defects on oxide-free surfaces. The bonding of aggressive chloride anions enhances in the same direction, but to a lesser extent. On oxide surfaces benzotriazole bonds considerably stronger to coordinatively unsaturated Cu sites. This suggests that benzotriazole is able to passivate the reactive under-coordinated surface sites that are plausible microscopic sites for corrosion attack.

The adsorption behavior of benzotriazole is non-trivial, because it can adsorb (at least in principle) in a variety of different forms. Perhaps this is one of the strengths of benzotriazole; depending on different conditions it adopts one of the several possible forms and thus sustains various situations. However, benzotriazole chemisorbs strongly only in deprotonated form. Gross bonding is even stronger when BTA is incorporated into BTA–Cu organometallic adcomplexes. DFT results are therefore consistent with experimental evidence that the ability of benzotriazole to inhibit corrosion is due to the formation of organometallic complexes. This readily explains why benzotriazole is more effective at higher pH values. Namely, at low pH (and low potentials) the BTA transforms to $BTAH_{(ads)}$,[47] which is bonded considerably weaker to the surface and may eventually desorb; according to the calculations the most probable adsorption form under such conditions is the BTAH physisorbed parallel to the surface and intermolecularly connected into H-bonding network with other BTAH molecules.¶

Strong inhibitor–surface bonding, as important as it may be, is by no means the only relevant factor for corrosion inhibition. $BTAH_\perp$ and $[BTA–Cu]_n$ considerably reduce the metal work function, which is a consequence of large per-

---

¶ Only deprotonated BTA⁻ and neutral BTAH were considered in this paper, because protonated $BTAH_2^+$ seems not to be competitive. According to DFT calculations, $BTAH_{2(ads)}$ bonds only marginally stronger than the neutral BTAH to Cu surfaces,[26] but it solvates considerably stronger (for further DFT-based analysis of the adsorption of deprotonated, neutral, and protonated azoles, see our recent study[36]). This implies that $BTAH_2^+$ prefers being solvated rather than adsorbed. It was reported that it is the dominant adsorbed form only at pH $\lesssim 0$.[62]

---

manent molecular dipole and properly oriented adsorption structure. It was argued that such a pronounced effect on the work function should *diminish* any reaction that donates electron(s) to the metal (*e.g.*, $Cl^-_{(solv)} \rightarrow Cl_{(ads)} + e^-$ or $Cu_{(solid)} \rightarrow Cu^{n+}_{(solv)} + ne^-_{(metal)}$). This reasoning is consistent with the fact that benzotriazole predominantly affects anodic reaction, although it is a mixed type inhibitor.[11,63] A large permanent molecular dipole is a general characteristic of azoles (*e.g.*, imidazole (3.8 D), triazole (4.4 D), tetrazole (5.4 D)).[4] A mechanism based on the reduction of work function may be therefore operative also for other azole inhibitors. There are, however, significant differences between imidazole and triazole/tetrazole based inhibitors. Our recent DFT calculations suggest that imidazoles are active against corrosion in neutral molecular form, while tetrazoles—similar to triazoles—inhibit the corrosion in their deprotonated form.[36] The reason for different behaviour of imidazoles is two fold; the first is due to their more basic nature and the second is related to their molecular spatial structure, because of which they can form only one strong N–Cu bond, while triazoles and tetrazole can form at least two.

An ability to form soluble complexes with dissolved metal ions as well as the solubility of standalone inhibitor are also relevant in the context of corrosion. A formation of soluble complexes between inhibitors and metal ions would help increase the dissolution of metal, thus having an effect of promoting the corrosion. This effect has been characterized for several imidazole based inhibitors in our parallel study.[64] As for the solubility, it is known that the more soluble is the molecule, the smaller is its (relative) affinity for adsorption.[3] Ideas of similar kind were very recently used by Mondal and Taylor,[65] who described a clever approach toward a rational design of corrosion inhibitors.

Last but not the least, the ability of a molecule to inhibit corrosion of metal is also given by the chemical nature of the metal itself, because molecules bond differently to various metals. For example, while Cu and Al are not reactive enough to interact with the azoles's π system,$^\parallel$ Fe can readily do so.[26] This can have a pronounced effect on the structure of adsorbed molecule.

Acknowledgements

References

1 M. M. Antonijević and M. B. Petrović, *Int. J. Electrochem. Sci.*, 2008, **3**, 1–28.
2 G. Schmitt, *Brit. Corros. J.*, 1984, **19**, 165–176.

$\parallel$ Cu can do it only exceptionally: an example is the *apparent* chem+phys form of Fig. 1b and even then the interaction is driven by the dispersive van der Waals forces.[6]

3   J. O. Bockris and A. K. N. Reddy, *Modern Electrochemistry*, Kluwer Academic/Plenum Publishers, New York, Boston, Dordrecht, London, Moscow, 2nd edn., 2000, vol. 2B.

4   N. Kovačević and A. Kokalj, *J. Phys. Chem. C*, 2011, **115**, 24189–24197.

5   Y. Jiang and J. B. Adams, *Surf. Sci.*, 2003, **529**, 428–442.

6   S. Peljhan and A. Kokalj, *Phys. Chem. Chem. Phys.*, 2011, **13**, 20408–20417.

7   A. Kokalj, S. Peljhan, M. Finšgar and I. Milošev, *J. Am. Chem. Soc.*, 2010, **132**, 16657–16668.

8   S. Peljhan, J. Koller and A. Kokalj, *J. Phys. Chem. C*, 2014, **118**, 933–943.

9   J. B. Cotton and I. R. Scholes, *Brit. Corros. J.*, 1967, **2**, 1–5.

10   G. W. Poling, *Corros. Sci.*, 1970, **10**, 359–37.

11   M. Finšgar and I. Milošev, *Corros. Sci.*, 2010, **52**, 2737–2749.

12   D. Chadwick and T. Hashemi, *Corros. Sci.*, 1978, **18**, 39–51.

13   R. F. Roberts, *J. Electron. Spectrosc.*, 1974, **4**, 273–291.

14   V. Brusic, M. A. Frisch, B. N. Eldridge, F. P. Novak, F. B. Kaufman, B. M. Rush and G. S. Frankel, *J. Electrochem. Soc.*, 1991, **138**, 2253–2259.

15   B.-S. Fang, C. G. Olson and D. W. Lynch, *Surf. Sci.*, 1986, **176**, 476–490.

16   G. Xue, J. Ding, P. Lu and J. Dong, *J. Phys. Chem.*, 1991, **95**, 7380–7384.

17   P. Giannozzi, S. Baroni, N. Bonini, M. Calandra, R. Car, C. Cavazzoni, D. Ceresoli, G. L. Chiarotti, M. Cococcioni, I. Dabo, A. D. Corso, S. de Gironcoli, S. Fabris, G. Fratesi, R. Gebauer, U. Gerstmann, C. Gougoussis, A. Kokalj, M. Lazzeri, L. Martin-Samos, N. Marzari, F. Mauri, R. Mazzarello, S. Paolini, A. Pasquarello, L. Paulatto, C. Sbraccia, S. Scandolo, G. Sclauzero, A. P. Seitsonen, A. Smogunov, P. Umari and R. M. Wentzcovitch, *J. Phys.: Condens. Matter.*, 2009, **21**, 395502.

18   D. Vanderbilt, *Phys. Rev. B*, 1990, **41**, 7892–7895.

19   A. Kokalj, *J. Mol. Graph. Model.*, 1999, **17**, 176–179.

20   J. P. Perdew, K. Burke and M. Ernzerhof, *Phys. Rev. Lett.*, 1996, **77**, 3865–3868.

21   S. Grimme, *J. Comput. Chem.*, 2006, **27**, 1787–1799.

22   V. Barone, M. Casarin, D. Forrer, M. Pavone, M. Sambi and A. Vittadini, *J. Comput. Chem.*, 2009, **30**, 934–939.

23   A. Kokalj and S. Peljhan, *Langmuir*, 2010, **26**, 14582–14593.

24   S. Peljhan and A. Kokalj, *J. Phys. Chem. C*, 2009, **113**, 14363–14376.

25   X. Chen and H. Häkkinen, *J. Phys. Chem. C*, 2012, **116**, 22346–22349.

26   N. Kovačević and A. Kokalj, *Mater. Chem. Phys.*, 2012, **137**, 331–339.

27   A. Kokalj, S. Peljhan and J. Koller, *J. Phys. Chem. C*, 2014, **118**, 944–954.

28   F. Grillo, D. W. Tee, S. M. Francis, H. A. Früchtl and N. V. Richardson, *J. Phys. Chem. C*, 2014, **118**, 8667–8675.

29   J. F. Walsh, H. S. Dhariwal, A. Gutirrez-Sosa, P. Finetti, C. A. Muryn, N. B. Brookes, R. J. Oldman and G. Thornton, *Surf. Sci.*, 1998, **415**, 423–432.

30   J. O. Nilsson, C. Tornkvist and B. Liedberg, *Appl. Surf. Sci.*, 1989, **37**, 306–326.

31   F. Grillo, D. W. Tee, S. M. Francis, H. Fruchtl and N. V. Richardson, *Nanoscale*, 2013, **5**, 5269–5273.

32   A. Kokalj, *Phys. Rev. B*, 2011, **84**, 045418.

33   J. O. Bockris, A. K. N. Reddy and M. Gamboa-Aldeco, *Modern Electrochemistry*, Kluwer Academic/Plenum Publishers, New York, Boston, Dordrecht, London, Moscow, 2nd edn., 2000, vol. 2A.

34   M. T. M. Koper and R. A. van Santen, *Surf. Sci.*, 1999, **422**, 118–131.

35   S. Trasatti, *Electrochim. Acta*, 1991, **36**, 1659–1667.

36   N. Kovačević and A. Kokalj, *Corros. Sci.*, 2013, **73**, 7–17.

37   A. Kokalj, *Chem. Phys.*, 2012, **393**, 1–12.

38   S. Trasatti and L. M. Doubova, *J. Chem. Soc., Faraday Trans.*, 1995, **91**, 3311–3325.

39   L. Doubova and S. Trasatti, *Electrochim. Acta*, 1997, **42**, 785–791.

40   C. D. Taylor, S. A. Wasileski, J.-S. Filhol and M. Neurock, *Phys. Rev. B*, 2006, **73**, 165402.

41   M. J. Weaver, *Appl. Surf. Sci.*, 1993, **67**, 147–159.

42   M. T. M. Koper, R. A. van Santen, S. A. Wasileski and M. J. Weaver, *J. Chem. Phys.*, 2000, **113**, 4392–4407.

43   S. A. Wasileski, M. T. M. Koper and M. J. Weaver, *J. Phys. Chem. B*, 2001, **105**, 3518–3530.

44   J. B. Cotton, Proceedings of the 2nd International Congress on Metallic Corrosion, New York,

USA, 1963, pp. 590–596.

45 J. C. Rubim, I. G. R. Gutz, O. Sala and W. J. Orville-Thomas, *J. Mol. Struct. (Theochem)*, 1983, **100**, 571–583.

46 D. Chadwick and T. Hashemi, *J. Electron. Spectrosc.*, 1977, **10**, 79–83.

47 R. Youda, H. Nishihara and K. Aramaki, *Electrochim. Acta*, 1990, **35**, 1011–1017.

48 Y. Jiang, J. B. Adams and D. Sun, *J. Phys. Chem. B*, 2004, **108**, 12851–12857.

49 S. Peljhan, *Ph.D. thesis*, University of Ljubljana, 2012.

50 S. Peljhan and A. Kokalj, 2015, in preparation.

51 V. Maurice and P. Marcus, *Electrochim. Acta*, 2012, **84**, 129–138.

52 M. M. Islam, B. Diawara, V. Maurice and P. Marcus, *Surf. Sci.*, 2009, **603**, 2087–2095.

53 J. Kunze, V. Maurice, L. H. Klein, H.-H. Strehblow and P. Marcus, *J. Phys. Chem. B*, 2001, **105**, 4263–4269.

54 V. Maurice, H.-H. Strehblow and P. Marcus, *Surf. Sci.*, 2000, **458**, 185–194.

55 A. Soon, M. Todorova, B. Delley and C. Stampfl, *Phys. Rev. B*, 2007, **75**, 125420.

56 A. Soon, M. Todorova, B. Delley and C. Stampfl, *Phys. Rev. B*, 2007, **76**, 129902.

57 A. Östen, M. Göthelid and U. O. Karlsson, *Surf. Sci.*, 2009, **603**, 257–264.

58 X. Nie, G. L. Griffin, M. J. Janik and A. Asthagiri, *Catal. Commun.*, 2014, **52**, 88–91.

59 P. W. Tasker, *J. Phys. C Solid State*, 1979, **12**, 4977–4984.

60 L. D. Hansen, B. D. West, E. J. Baca and C. L. Blank, *J. Am. Chem. Soc.*, 1968, **90**, 6588–6592.

61 M. Finšgar, J. Kovač and I. Milošev, *J. Electrochem. Soc.*, 2010, **157**, C52–C60.

62 H. Y. H. Chan and M. J. Weaver, *Langmuir*, 1999, **15**, 3348–3355.

63 M. Finšgar, A. Lesar, A. Kokalj and I. Milošev, *Electrochim. Acta*, 2008, **53**, 8287–8297.

64 N. Kovačević, I. Milošev and A. Kokalj, 2015, in preparation.

65 S. K. Mondal and S. R. Taylor, *J. Electrochem. Soc.*, 2014, **161**, C476–C485.

Faraday Discussions
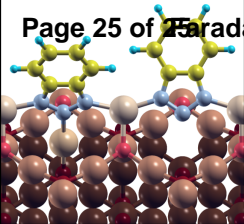
Tentative structure of polymeric organometallic complex between benzotriazole and copper on the surface of Cu₂O as predicted by DFT calculations.